CCD Photometry and Roche Modeling of the Eclipsing Deep Low Mass, Overcontact Binary Star System TYC 2058-753-1

Kevin B. Alton
UnderOak Observatory, 70 Summit Avenue, Cedar Knolls, NJ; kbalton@optonline.net

Received October 6, 2016; revised February 12, 2018; accepted March 27, 2018

Abstract TYC 2058-753-1 (NSVS 7903497; ASAS 165139+2255.7) is a W UMa binary system (P = 0.353205 d) which has not been rigorously studied since first being detected nearly 15 years ago by the ROTSE-I telescope. Other than the unfiltered ROTSE-I and monochromatic All Sky Automated Survey (ASAS) survey data, no multi-colored light curves (LC) have been published. Photometric data collected in three bandpasses (B, V, and I_c) at Desert Bloom Observatory in June 2017 produced six times-of-minimum for TYC 2058-753-1 which were used to establish a linear ephemeris from the first directly measured Min I epoch (HJD_0). No published radial velocity data are available for this system, however, since this W UMa binary undergoes a very obvious total eclipse, Roche modeling produced a well-constrained photometric value for the mass ratio ($q_{ph} = 0.103 \pm 0.001$). This low-mass ratio binary star system also exhibits a high degree of contact ($f > 56\%$). There is a suggestion from the ROTSE-I and ASAS survey data as well as from the new LCs reported herein that maximum light during quadrature (Max I and Max II) is often not equal. As a result, Roche modeling of the TYC 2058-753-1 LCs was investigated with and without surface spots to address this asymmetry as well as a diagonally-aligned flat bottom during Min I that was observed in 2017.

1. Introduction

The variable behavior of TYC 2058-753-1 was first observed during the ROTSE-I CCD survey (Akerlof *et al.* 2000; Wozniak *et al.* 2004; Gettel *et al.* 2006) and subsequently confirmed from additional photometric measurements taken by the ASAS surrvey (Pojmański *et al.* 2005). The system was classified as an overcontact binary by Hoffman *et al.* (2009). Other than the sparsely sampled photometric readings from the ROTSE-I and ASAS surveys, no other LCs from this binary system were found in the literature. TYC 2058-753-1 is also included in a survey of 606 contact binaries from which accurate colors (BVR_cI_c) were derived (Terrell *et al.* 2012). The paper herein marks the first robust determination of an orbital period and its corresponding linear ephemeris to be published.

Deep, low mass ratio (DLMR) overcontact systems like TYC 2058-753-1 embody a subgroup of W UMa variables with mass ratios (m_2 / m_1) less than 0.25 and degrees of contact (f) greater than 50% (Yang and Qian 2015). Accordingly, these binary systems are approaching a final evolutionary stage before merging into single rapidly-rotating objects such as blue-straggler or FK Com-type stars. DLMR stars are considered an important astrophysical laboratory for studying the dynamical evolution of short-period binary stars in very close contact. In this regard, the Roche-type modeling of TYC 2058-753-1 contained within offers the first published study in which the physical and geometric elements of this system are derived.

2. Observations and data reduction

2.1. Photometry

The equipment at Desert Bloom Observatory (DBO) located in Benson, Arizona, includes a 0.4-m catadioptic telescope mounted on an equatorial fork with an SBIG STT-1603 ME CCD camera installed at the Cassegrain focus. This f/6.7 instrument produces a 17.4 × 11.6 arcmin field-of-view with a 1.36 arcsec/pixel scale (binned 2 × 2). Automated imaging was performed with Astrodon photometric B, V, and I_c filters manufactured to match the Bessell prescription. The computer clock was updated immediately prior to each session and exposure time for all images adjusted to 75 sec. Image acquisition (lights, darks, and flats) was performed using MAXIMDL version 6.13 (Diffraction Limited 2016) or THESKYX version 10.5.0 (Software Bisque 2013) while calibration and registration were performed with AIP4WIN v2.4.0 (Berry and Burnell 2005). MPO CANOPUS v10.7.1.3 (Minor Planet Observer 2015) provided the means for further photometric reduction to LCs using a fixed ensemble of four non-varying comparison stars in the same field-of-view (FOV). Error due to differential refraction and color extinction was minimized by only using data from images taken above 30° altitude (airmass < 2.0). Instrumental readings were reduced to catalog-based magnitudes using the reference MPOSC3 star fields built into MPO CANOPUS (Warner 2007).

2.2. Light curve analyses

Roche type modeling was performed with WDWINT v5.6a (Nelson 2009) and PHOEBE 0.31a (Prša and Zwitter 2005), both of which employ the Wilson-Devinney (W-D) code (Wilson and Devinney 1971; Wilson 1990). Spatial models of TYC 2058-753-1 were rendered with BINARY MAKER 3 (BM3; Bradstreet and Steelman 2002) once W-D model fits were finalized. Times-of-minimum were calculated using the method of Kwee and van Woerden (1956) as implemented in PERANSO v2.5 (Vanmunster 2006).

3. Results and discussion

3.1. Photometry and ephemerides

The four stars in the same FOV with TYC 2058-753-1 (Table 1) which were used to derive MPOSC3-based magnitudes showed no evidence of inherent variability over the interval of image acquisition and stayed within ± 0.007 mag for V–and I_c–and ± 0.017 for B-passbands. Photometric values in B (n = 464), V (n = 478), and I_c (n = 474) were folded by period analysis to generate three LCs that spanned 16 days between June 3 and

Table 1. Astrometric coordinates (J2000) and color indices (B–V) for TYC 2058-0753-1 and four comparison stars used in this photometric study.

Star Identification	*R.A. (J2000)* *h m s*	*Dec. (J2000)* *° ′ ″*	*MPOSC3[a] (B–V)*
TYC 2058-0753-1	16 51 39.43	22 55 43.5	0.822
GSC 2058-0807	16 52 02.94	22 54 10.3	0.743
GSC 2058-0583	16 52 05.65	22 57 16.9	0.674
GSC 2058-0841	16 52 42.02	22 57 16.9	0.463
2MASS 16515918+2256394	16 51 59.06	22 56 39.0	0.387

a. MPOSC3 is a hybrid catalog (Warner 2007) which includes a large subset of the Carlsberg Meridian Catalog (CMC-14) as well as from the Sloan Digital Sky Survey (SDSS).

June 19, 2017 (Figure 1). In total, four primary (p) and two secondary (s) minima were captured during this investigation; the corresponding data (B, V, and I_c) were averaged from each session (Table 2) since no color dependency on the timings was noted. Initially a period determination was made from survey data (ROTSE-I and ASAS) collected between 1999–2009 using PERANSO v2.5 (Vanmunster 2006). The selected analysis method employs periodic orthogonal polynomials (Schwarzenberg-Czerny 1996) to fit observations and analysis of variance (ANOVA) to evaluate fit quality. The resulting orbital period (P = 0.353206 ± 0.000008 d) was very similar to the value cited at the International Variable Star Index website (Watson *et al.* 2014). The Fourier routine (FALC; Harris *et al.* 1989) in MPO CANOPUS provided a comparable period solution (0.353205 ± 0.000001 d) using only the multicolor data from DBO. Finally, after converting magnitude to normalized flux, ROTSE-I, ASAS, and DBO light curve data (HJD; V mag) were then folded together; the best fit was found where the orbital period was 0.353205 ±0.000008 d (Figure 2). As expected with so few data, eclipse timing differences when plotted against period cycle number did not provide any evidence for period change (Figure 3). The first epoch (HJD_0) for this eclipsing binary is therefore defined by the following linear ephemeris equation:

$$\text{Min. I (hel.)} = 2457909.7566\ (3) + 0.353205\ (8)\ E. \quad (1)$$

There is an expectation that while DLMR systems slowly collapse into a higher degree of contact before merger, the orbital period will concomitantly decrease. Since this result is not demonstrably obvious after folding the sparsely sampled survey data (1999–2009) with high cadence LC data acquired in 2017, this hypothesis may not be proven until many more years of eclipse timing data have been collected to determine whether the orbital period of this system undergoes change(s) with time.

3.2. Light curve behavior

LCs (Figure 1) exhibit minima which are separated by 0.5 phase and are consistent with synchronous rotation in a circular orbit typified by W UMa-type variable stars. The flattened bottom at Min I is diagnostic of a binary system that undergoes a total eclipse. Interestingly, LC data from the ROTSE-I and ASAS surveys (Figure 2) exhibit significant variability around Min II suggesting that the deepest minimum likely alternates from time-to-time. The 2017 LCs exhibit asymmetry during

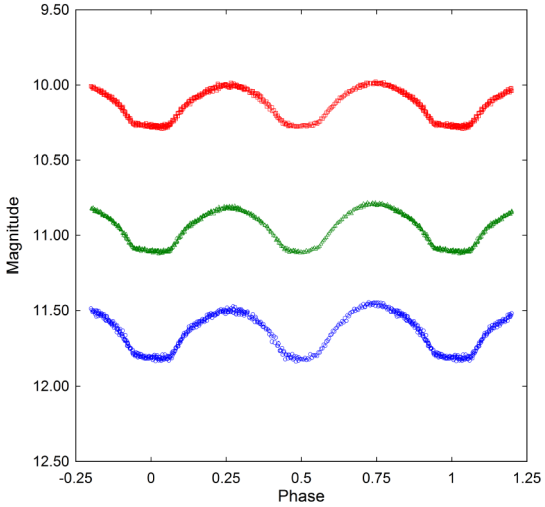

Figure 1. CCD-derived light curves for TYC 2058-753-1 produced from photometric data obtained between June 3 and June 19, 2017. The top (I_c; n = 474), middle (V; n = 478), and bottom curve (B; n =464) shown above were reduced to MPOSC3-based catalog magnitudes using MPO CANOPUS.

Table 2. New times-of-minimum for TYC 2058-753-1 acquired at Desert Bloom Observatory.

ToM HJD–2400000	*UT ± Error*	*Observation Date*	*Type of Minimum[a]*
57909.7566	0.0003	05 June 2017	p
57915.7595	0.0001	11 June 2017	p
57917.6978	0.0002	13 June 2017	s
57921.7631	0.0002	17 June 2017	p
57923.7032	0.0002	19 June 2017	p
57923.8823	0.0002	19 June 2017	s

a. s = secondary; p = primary.

quadrature such that Max I is fainter than Max II (Figure 1). This effect often attributed to O'Connell (1951) has been variously ascribed to the presence of cool starspot(s), hot region(s), gas stream impact on either or both of the binary stars, and/or other unknown phenomena which produce surface inhomogeneities (Yakut and Eggleton 2005). The net result can be unequal heights during maximum light and is often simulated by the introduction of starspots during Roche-type modeling of the LC data.

3.3. Spectral classification

Interstellar extinction (A_V) was estimated using a program (ALEXTIN) developed by Amôres and Lépine (2005) for targets within the Milky Way Galaxy (MWG). In addition to the galactic coordinates (*l, b*) an estimated distance (kpc) to each target is required. The dust maps generated by Schlegel *et al.* (1998) and later adjusted by Schlafly and Finkbeiner (2011) determine extinction based on total dust in a given direction without regard to the target distance. This often leads to an overestimation of reddening within the MWG, most commonly determined as $E(B–V) = A_V / 3.1$. As will be described in section 3.7, the distance to overcontact binary stars can be estimated based on a number of different approaches even in the absence of a directly determined parallax. In this case the adopted

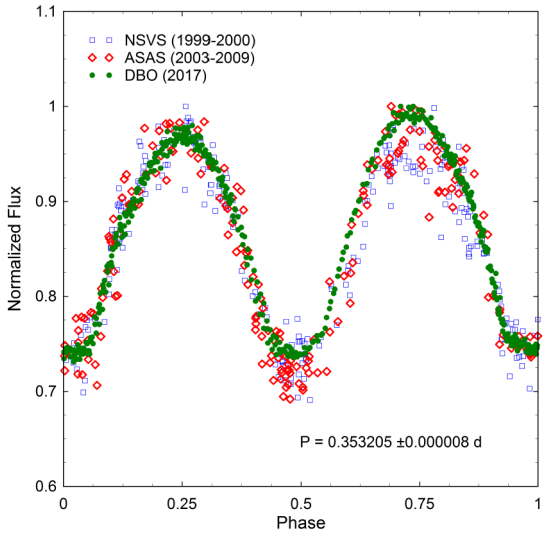

Figure 2. Survey data from the ROTSE-I telescope (NSVS), ASAS Survey, and photometric results (HJD; Vmag) collected at DBO were folded together using period analysis (P = 0.353205 ± 0.000008 d). Greater scatter at phase = 0.50 and 0.75 suggests the presence of an active surface for TYC 2058-753-1.

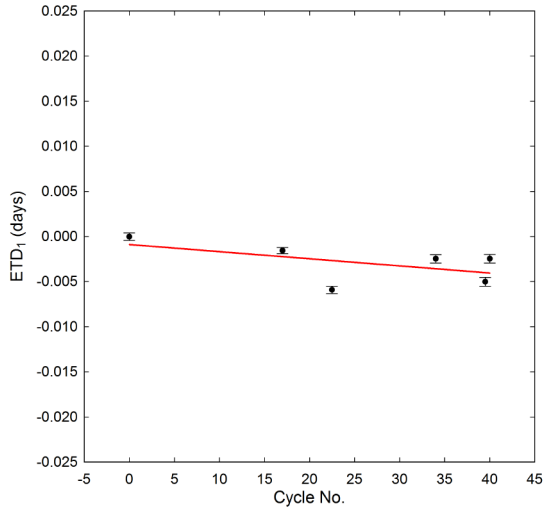

Figure 3. Linear fit of eclipse timing differences (ETD_1) and period cycle number for TYC 2058-0753-1 captured at DBO over 16 days.

Table 3. Spectral classification of TYC 2058-753-1 based upon dereddened (B–V) data from four surveys and the present study.

	Terrell et al. *2005*	*2MASS*	*USNO-A2*	*UCAC4*	*Present Study*
$(B–V)_0$	0.728	0.815	0.774	0.770	0.667
T_{eff1}[a](K)	5506	5282	5353	5370	5703
Spectral Class[a]	G7-G8V	G9-K0V	G8-G9V	G8-G9V	G3-G4V

a. T_{eff1} interpolated and main sequence spectral class assigned from Pecaut and Mamajek (2013). Median value, $(B–V)_0$ = 0.770 ± 0.042, corresponds to a G8V-G9V primary star (T_{eff1} = 5370 K).

distance (~0.190 kpc) results in a reddening value (E(B–V)) of 0.0074 ± 0.0004. Color index (B–V) data collected at DBO and those acquired from an ensemble of four other sources (Table 3) were subsequently dereddened. The median result ($(B-V)_0$ = 0.770 ± 0.042) points to a main sequence primary star with an effective temperature (5370 K) that ranges in spectral type between G8V and G9V (Pecaut and Mamajek 2013).

3.4. Roche modeling approach

Perhaps the greatest obstacle to definitively characterizing the absolute dimensions, geometry, and mass of an eclipsing pair of stars is the general lack of RV data for relatively dim (Vmag > 12) binary systems. This situation is likely to continue until mitigated by the final release of spectroscopic data from the Gaia Mission in 2022. Without RV data, it is not possible to unequivocally determine the mass ratio ($q = m_2/m_1$), total mass or whether TYC 2058-753-1 is an A- or W-type overcontact binary system. Nonetheless, a reliable photometric value for mass ratio (q_{ph}) can be determined but only for those W UMa systems where a total eclipse is observed (Terrell and Wilson 2005). Secondly, in many cases an educated guess about the W UMa subtype (A- or W-) can be made based on general characteristics of each overcontact binary system. Binnendijk (1970) defined an A-type W UMa variable as one in which the deepest minimum (Min I) results from the eclipse of the hotter more massive star by the cooler less massive cohort. By contrast W-types exhibit the deepest minimum when the hotter, but less massive star is eclipsed by its more massive but cooler companion. The published record is very clear that the majority (39 of 46) of DLMR binaries studied thus far appear to be A-type systems (Yang and Qian 2015). By and large, A-type W UMa variables can be characterized by their total mass ($M_T > 1.8\,M_\odot$), spectral class (A-F), orbital period (P > 0.4 d), high degree of thermal contact(f), tendency to totally eclipse due to large size differences, mass ratio (q < 0.3), and the temperature difference ($\Delta T < 100$ K) between the hottest and coolest star (Skelton and Smits 2009). In this case, TYC 2058-753-1 shares attributes from both A- and W-types thereby complicating a definitive assignment without having RV data. Furthermore, LC data from the ASAS (Pojmański *et al.* 2005) and ROTSE surveys survey (Akerlof *et al.* 2000; Gettel *et al.* 2006) suggest that Min I, the deepest minimum, alternates with Min II over time as might be expected from a heavily spotted system. This behavior has been reported for other DMLR overcontact binaries including EM Psc (Qian *et al.* 2008), V1191 Cyg (Ulaş *et al.* 2012), FG Hya (Qian and Yang 2005), and GR Vir (Qian and Yang 2004). Roche modeling of LC data from TYC 2058-753-1 was initially accomplished using the program PHOEBE 0.31a (Prša and Zwitter 2005). The model selected was for an overcontact binary (Mode 3); weighting for each curve was based upon observational scatter. Bolometric albedo ($A_{1,2} = 0.5$) and gravity darkening coefficients ($g_{1,2} = 0.32$) for cooler stars (< 7500 K) with convective envelopes were respectively based on the seminal work of Ruciński (1969) and Lucy (1967). The effective temperature of the more massive primary star was fixed ($T_{eff1} = 5370$ K) according to the earlier designation as spectral type G8V to G9V. Logarithmic limb darkening coefficients (x_1, x_2, y_1, y_2) were interpolated according

to Van Hamme (1993) after any adjustment in the secondary (T_{eff2}) effective temperature. Except for T_{eff1}, $A_{1,2}$, and $g_{1,2}$, all other parameters were allowed to vary during DC iterations. Roche modeling was initially seeded with q = 0.150 and i = 89° based on the similarity between orbital period, effective temperature (T_{eff1}), and light curves for TYC 2058-753-1 and EM Psc (González-Rojas *et al.* 2003; Qian *et al.* 2008). The fit with a slightly higher (+100 K) effective temperature for the secondary was initially investigated since the smaller but potentially hotter star appeared to be occulted at Min I in 2017. This assessment included synthesis of LCs for TYC 2058-753-1 with and without the incorporation of spot(s) to address the negative O'Connell effect (Max II brighter than Max I) and the flattened but diagonally aligned bottom during Min I.

3.5. Roche modeling results

The initial estimates (PHOEBE 0.31a) for q, i, and T_{eff2} converged to a Roche model solution in which the effective temperature of the less massive secondary proved to be slightly higher (> 24 K) than the primary star. Thereafter, final values and errors for T_{eff2}, i, q, $\Omega_{1,2}$, and the spot parameters were determined using WDWINT v5.6a (Table 4). Corresponding unspotted (Figure 4) and spotted (Figure 5) LC simulations revealed that the addition of a cool spot on the primary and a hot spot on the secondary was necessary to achieve the best fit (χ^2) for these multi-color data. Pictorial models rendered (BM3) with both spots using the physical and geometric elements from the 2017 LCs (V-mag) are shown in Figure 6. In this case, these results are consistent with those expected from a W-type overcontact binary system. Nonetheless, it is very clear from the ROTSE-I and ASAS survey data that the deepest minimum for TYC 2058-753-1 can alternate; this most likely occurs due to significant changes in spot location and/or temperature. A subset of LC data (2005–2007) collected during the ASAS survey (Pojmański *et al.* 2005) offers further insight into the challenges faced with trying to unambiguously define this system without supporting RV data. Although the Roche model parameter estimates are more variable (Table 4) from the ASAS survey data, the results suggest that Min I (Figure 7) could arise from a transit of the secondary across the face of the primary star (Figure 8). This scenario is essentially the definition of an A-type W UMa-type system and different from the 2017 findings. Interestingly, the best solution for the 2005–2007 data suggests that the secondary is also hotter (110 K) than the primary, an outcome reported for a large fraction (8/39) of A-type DLMR overcontact binaries (Yang and Qian 2015). The fill-out parameter (f), which is a measure of the shared outer surface volume between each star, was calculated according to Bradstreet (2005) as:

$$f = (\Omega_{inner} - \Omega_{1,2}) / (\Omega_{inner} - \Omega_{outer}), \quad (2)$$

where Ω_{outer} is the outer critical Roche equipotential, Ω_{inner} is the value for the inner critical Roche equipotential, and $\Omega = \Omega_{1,2}$ denotes the common envelope surface potential for the binary system. Since the fill-out value ($f > 0.56$) for TYC 2058-753-1 lies between $0 < f < 1$, the system is defined as an overcontact binary. This high degree of contact in combination with the

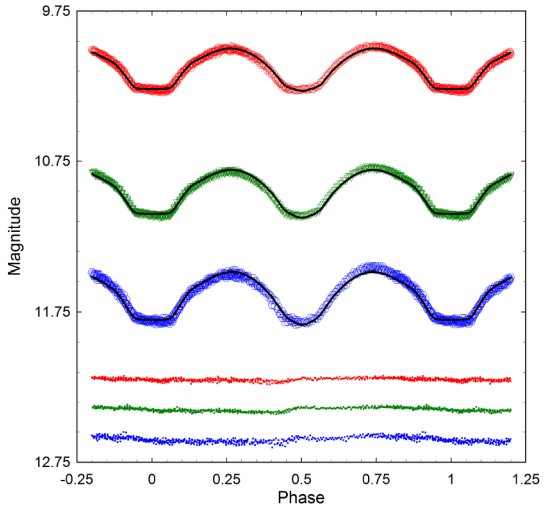

Figure 4. TYC 2058-753-1 Roche model fits (solid-line) of LCs (B-, V-, and I_c-mag) produced from CCD data collected at DBO during 2017. This analysis assumed a W-subtype overcontact binary with no spots; residuals from the model fits are offset at the bottom of the plot to keep the values on scale.

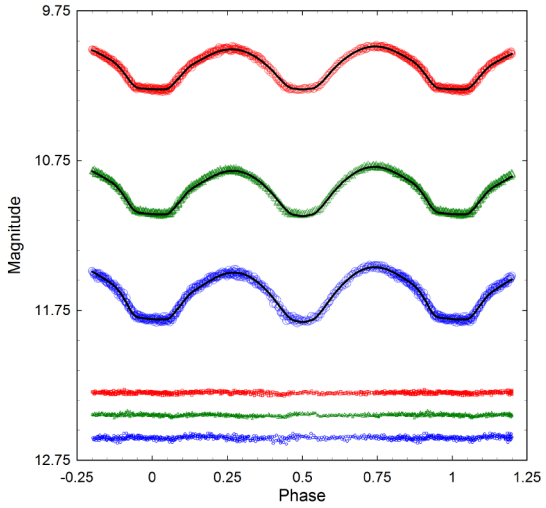

Figure 5. TYC 2058-753-1 Roche model fits (solid-line) of LCs (B-, V-, and I_c-mag) produced from CCD data collected at DBO during 2017. This analysis assumed a W-subtype overcontact binary with a cool spot on the primary and a hot spot on the secondary star; residuals from the model fits are offset at the bottom of the plot to keep the values on scale.

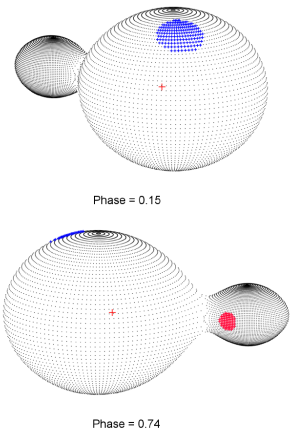

Figure 6. Spatial renderings of TYC 2058-753-1 generated from photometric data (V-mag) acquired in 2017 showing putative locations of a cool spot (blue) on the primary star and a hot spot (red) on the secondary star.

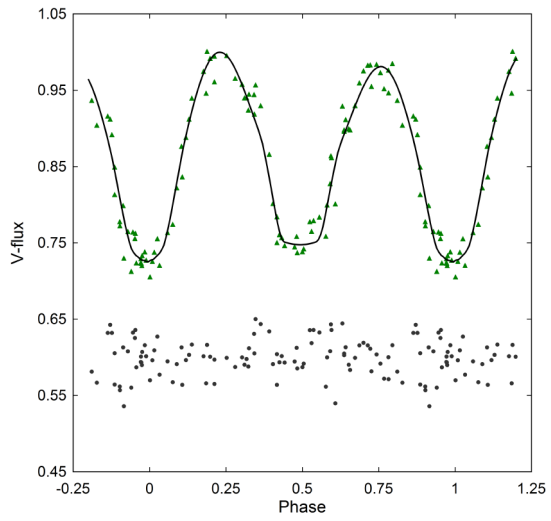

Figure 7. Roche model fit (solid-line) of ASAS survey data for TYC 2058-753-1 acquired between 2005 and 2007. The positive O'Connell effect (Max I > Max II) was simulated by the addition of a cool spot on the less massive secondary component.

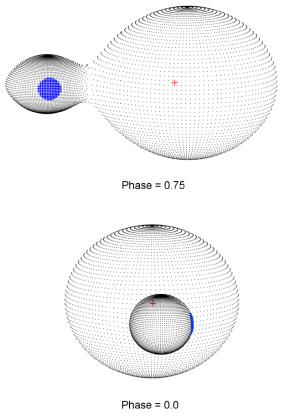

Figure 8. Spatial renderings of TYC 2058-753-1 generated from ASAS photometric data (2005–2007) showing putative location of a cool spot (blue) on the secondary star.

photometrically determined mass ratio ($q_{ph}=0.103\pm0.001$) meets the criteria for what is considered a deep, low mass ratio (DLMR) overcontact binary system. With the exception of AH Cnc, which is a clear outlier, analysis of 23 other DLMR systems (Yang and Qian 2015) shows a strong correlation ($r=0.94$) between spectrophotometric (q_{sp}) and photometric (q_{ph}) mass ratios when both are reported. This is by no means a substitute for having RV data, but it does point out that the q_{ph} value reported herein will likely compare favorably with a more rigorous spectrophotometric determination in the future.

3.6. Absolute parameters

Preliminary absolute parameters (Table 5) were derived for each star in this system using results from the best fit simulation (spotted model) of the 2017 LC. In the absence of RV data, total mass can not be unequivocally calculated; however, stellar mass and radii estimates from binary systems have been tabulated over a wide range of spectral types. This includes a value ($M_1 = 0.98\pm0.05\,M_\odot$) interpolated from Harmanec (1988) and another ($M_1=0.93\pm0.03\,M_\odot$) from Pecaut and Mamajek (2013). Additionally, two different empirical period-mass relationships for W UMa-binaries have been published, by Qian (2003) and later by Gazeas and Stępień (2008). According to Qian (2003) the mass of the primary star (M_1) can be determined from Expression 3:

$$\log M_1 = (0.761\pm0.150)\log P + (1.82\pm0.28), \quad (3)$$

where P is the orbital period in days and leads to $M_1=1.08\pm0.08\ M_\odot$ for the primary. The other mass-period relationship (Equation 4) derived by Gazeas and Stępień (2008):

$$\log M_1 = (0.755\pm0.059)\log P + (0.416\pm0.024), \quad (4)$$

corresponds to a W-type W UMa system where $M_1=1.19\pm0.10\,M_\odot$. The median of all values ($M_1=1.03\pm0.08\ M_\odot$) was used for subsequent determinations of M_2, semi-major axis (a), volume-radius (r_L), bolometric magnitude (M_{bol}), and distance (pc) to TYC 2058-753-1. The semi-major axis, $a(R_\odot)=2.20\pm0.05$, was calculated according to Kepler's third law (Equation 5) where:

$$a^3 = (G\times P^2(M_1+M_2))/(4\pi^2). \quad (5)$$

According to Equation 6 derived by Eggleton (1983), the effective radius of each Roche lobe (r_L) can be calculated to within an error of 1% over the entire range of mass ratios ($0<q<\infty$):

$$r_L = (0.49q^{2/3})/(0.6q^{2/3}+ln(1+q^{1/3})). \quad (6)$$

Volume-radius values were detemined for the primary ($r_1=0.5761\pm0.0003$) and secondary ($r_2=0.2084\pm0.0002$) stars. The absolute solar radii for both binary constituents can then be calculated where $R_1=a\times r_1=1.27\pm0.03\,R_\odot$ and $R_2=a\times r_2=0.46\pm0.01\,R_\odot$. The bolometric magnitude ($M_{bol1,2}$) and luminosity in solar units ($L_\odot$) for the primary and secondary stars were calculated from well-known relationships where:

$$M_{bol1,2} = 4.75 - 5\log(R_{1,2}/R_\odot) - 10\log(T_{1,2}/T_\odot), \quad (7)$$

and

$$L_{1,2} = (R_{1,2}/R_\odot)2\,(T_{1,2}/T_\odot)^4. \quad (8)$$

Assuming that $T_{eff1}=5370\,K$, $T_{eff2}=5394\,K$, and $T_\odot=5772\,K$, the bolometric magnitudes are $M_{bol1}=4.55\pm0.05$ and $M_{bol1}=6.74\pm0.05$, while the solar luminosities for the primary and secondary are $L_1=1.20\pm0.05\,L_\odot$ and $L_2=0.16\pm0.01\,L_\odot$, respectively.

3.7. Distance estimates to TYC 2058-753-1

Using the data generated at DBO, the distance to TYC 2058-753-1 was estimated (183 ± 11 pc) from the distance modulus equation (9) corrected for interstellar extinction:

$$d(pc) = 10^{(m-M_v-A_v+5)/5}, \quad (9)$$

Table 4. Light curve parameters employed for Roche modeling and the geometric elements determined when assuming that TYC 2058-753-1 is an A-type overcontact (2005–2007) or a W-type overcontact binary (2017).

Parameter	*No Spot (2017)*	*Spotted (2017)*	*Spotted (2005–2007)*
T_{eff1} (K)[a]	5370	5370	5370
T_{eff2} (K)[b]	5481 ± 6	5394 ± 4	5511 ± 52
q (m_2 / m_1)[b]	0.102 ± 0.001	0.103 ± 0.001	0.101 ± 0.002
A[a]	0.5	0.5	0.5
g[a]	0.32	0.32	0.32
$\Omega_1 = \Omega_2$[b]	1.928 ± 0.001	1.924 ± 0.002	1.904 ± 0.012
i°[b]	80.13 ± 0.22	78.07 ± 0.16	80.6 ± 3.3
$A_P = T_S / T$[c]	—	0.89 ± 0.01	—
Θ_P (spot co-latitude)	—	35.4 ± 0.3	—
φ_P[c] (spot longitude)	—	133.7 ± 0.5	—
r_P[c] (angular radius)	—	16.2 ± 0.1	—
$A_S = T_S / T$	—	1.18 ± 0.01	0.69 ± 0.21
Θ_S (spot co-latitude)	—	90 ± 2.5	90 ± 20
φ_S (spot longitude)	—	58.3 ± 1.3	270 ± 42
r_S (angular radius)	—	15.0 ± 0.2	20.0 ± 2.1
$L_1 / (L_1 + L_2)_B$[b,d]	0.8575 ± 0.0002	0.8679 ± 0.0001	—
$L_1 / (L_1 + L_2)_V$	0.8639 ± 0.0001	0.8707 ± 0.0001	0.8554 ± 0.0005
$L_1 / (L_1 + L_2)_{I_c}$	0.8689 ± 0.0001	0.8726 ± 0.0001	—
r_1[b] (pole)	0.5452 ± 0.0002	0.5440 ± 0.0001	0.5510 ± 0.0033
r_1 (side)	0.6138 ± 0.0007	0.6118 ± 0.0001	0.6236 ± 0.0057
r_1 (back)	0.6354 ± 0.0008	0.6329 ± 0.0002	0.6467 ± 0.0065
r_2[b] (pole)	0.2068 ± 0.0019	0.2045 ± 0.0008	0.2127 ± 0.0104
r_2 (side)	0.2173 ± 0.0024	0.2146 ± 0.0010	0.2247 ± 0.0131
r_2 (back)	0.2730 ± 0.0078	0.2657 ± 0.0031	0.3060 ± 0.0829
Filling factor	56.5%	64.0%	90%
χ^2 (B)[e]	0.03074	0.01179	—
χ^2 (V)[e]	0.05511	0.01899	0.04609
χ^2 (I_c)[e]	0.14611	0.07703	—

a. Fixed during differential corrections (DC).
b. Error estimates for q_{ph}, i, $\Omega_1 = \Omega_2$, T_{eff2}, $L_1 / (L_1 + L_2)$, spot parameters, r_1, and r_2 (pole, side, and back) from WDWINT v5.6a (Nelson 2009).
c. Primary and secondary spot temperature (A_P; A_S); location (Θ_P,φ_P;Θ_S,φ_S) and size (r_P;r_S)parameters in degrees.
d. Bandpass dependent fractional luminosity; L_1 and L_2 refer to luminosities of the primary and secondary stars, respectively.
e. Monochromatic best Roche model fits (χ^2) from PHOEBE 0.31a (Prša and Zwitter 2005).

Table 5. Preliminary absolute parameters for TYC~2058-753-1 using results from the 2017 spotted Roche model.

Parameter	*Primary*	*Secondary*
Mass ($M_\odot$)	1.03 ± 0.08	0.11 ± 0.01
Radius ($R_\odot$)	1.27 ± 0.03	0.46 ± 0.01
a ($R_\odot$)	2.20 ± 0.05	—
Luminosity ($L_\odot$)	1.20 ± 0.05	0.16 ± 0.01
M_{bol}	4.55 ± 0.05	6.74 ± 0.05
Log(g)	4.25 ± 0.04	4.14 ± 0.04

In this case V_{avg} (m = 10.96 ± 0.11) was used rather than V-mag at Min I since during this time the primary star surface facing the observer is contaminated with a cool spot. M_V is the absolute magnitude derived using the bolometrically corrected magnitude ($M_{bol1} - BC = 4.62 \pm 0.05$), and the interstellar extinction ($A_V = 0.023 \pm 0.001$) was determined as described in section 3.3. Empirical relationships derived from calibrated models for overcontact binaries have also been used to approximate astronomical distances (pc). Mateo and Ruciński (2017) recently developed a relationship between orbital period ($0.275 < P < 0.575$ d) and distance (Tycho-Gaia Astronomic Solution parallax data) from a subset of contact binaries which showed that the absolute magnitude (M_V) can be estimated using expression (10):

$$M_V = (-8.67 \pm 0.65)(\log(P) + 0.4) + (3.73 \pm 0.06). \quad (10)$$

Accordingly the absolute magnitude was calculated to be $M_V = 4.181 \pm 0.069$. Substitution back into Equation 9 yields a distance of 224 ± 14 pc. Another value for distance (167 ± 22 pc) was calculated using Equation 11:

$$\log(d) = 0.2\, V_{max} - 0.18 \log(P) - 1.6\,(J-H) + 0.56, \quad (11)$$

derived by Gettel *et al.* (2006) from a ROTSE-I catalog of overcontact binary stars where d is distance in parsecs, P is the orbital period in days, $V_{max} = 10.81 \pm 0.01$, and (J–H) is the 2MASS color for TYC 2058-753-1. The combined mean distance to this system is therefore estimated to be 191 ± 9 pc.

4. Conclusions

CCD-derived light curves captured in B, V, and I_c passbands produced six new times-of-minimum for the largely ignored W UMa binary system TYC 2058-753-1. A first epoch (HJD_0) linear ephemeris for TYC 2058-753-1 was established, however,

a rigorous assessment of any eclipse timing differences is not possible without many more years of data. There is an expectation that TYC 2058-753-1, like many other DLMR systems, will eventually show a decrease in the orbital period as the binary components collapse into a single rapidly rotating star. An ensemble of reddening corrected (B–V) values from this study and other surveys suggests that the effective temperature of the most luminous star approximates 5370 K, which corresponds to G8V-G9V spectral class. The paucity of published RV data to unambiguously determine a mass ratio (q), total mass, and subtype (A or W) continues to challenge the definitive Roche modeling of newly discovered but relatively dim W UMa binaries. Fortunately this system experiences a clearly defined total eclipse at Min I which helps to constrain a photometrically determined mass ratio result ($q_{ph} = 0.103 \pm 0.001$). Spotted solutions were necessary to achieve the best Roche model fits for TYC 2058-753-1. LCs observed between 1999 and 2009 exhibit similar asymmetry at maximum light in addition to Min I and Min II switching relative to a reference epoch; this suggests that TYC 2058-753-1 has a very active surface. Furthermore, the highly variable nature of these LCs undermines any convincing attempt to define this system as a W-type or A-type overcontact system. Until which time RV data become available, any absolute parameters derived herein for this W UMa binary are subject to greater uncertainty. Public access to the photometric data (B, V, and I_c) acquired in 2017 can be found in the AAVSO International Database at the AAVSO website (https://www.aavso.org/data-download).

5. Acknowledgements

This research has made use of the SIMBAD database, operated at Centre de Données astronomiques de Strasbourg, France, the Northern Sky Variability Survey hosted by the Los Alamos National Laboratory, the All Sky Automated Survey hosted by Astronomical Observatory of the University of Warsaw, and the International Variable Star Index maintained by the AAVSO. The diligence and dedication shown by all associated with these organizations is much appreciated. A special thanks to the *JAAVSO* Editorial staff and the anonymous referee for their support and valuable input.

References

Akerlof, C., *et al.* 2000, *Astron. J.*, **119**, 1901.

Amôres, E. B., and Lépine, J. R. D. 2005, *Astron. J.*, **130**, 650.

Berry, R., and Burnell, J. 2005, *The Handbook of Astronomical Image Processing*, 2nd ed., Willmann-Bell, Richmond, VA.

Binnendijk, L. 1970, *Vistas Astron.*, **12**, 217.

Bradstreet, D. H. 2005, in *The Society for Astronomical Sciences 24th Annual Symposium on Telescope Science*, Society for Astronomical Sciences, Rancho Cucamonga, CA, 23.

Bradstreet, D. H., and Steelman D. P. 2002, *Bull. Amer. Astron. Soc.*, **34**, 1224.

Diffraction Limited. 2016, MAXIMDL version 6.13 image processing software (http://www.cyanogen.com).

Eggleton, P. P. 1983, *Astrophys. J.*, **268**, 368.

Gazeas, K. and Stcępień, K. 2008, *Mon. Not. Roy. Astron. Soc.*, **390**, 1577.

Gettel, S. J., Geske, M. T., and McKay, T. A. 2006, *Astron. J.*, **131**, 621.

González-Rojas, D. J., Castellano-Roig, J., Dueñas-Becerril, M., Lou-Felipe, M., Juan-Samso, J., and Vidal-Sainz, J. 2003, *Inf. Bull. Var. Stars*, No. 5437, 1.

Harmanec, P. 1988, *Bull. Astron. Inst. Czechoslovakia*, **39**, 329.

Harris, A. W., *et al.* 1989, *Icarus*, **77**, 171.

Hoffman, D. J., Harrison, T. E., and McNamara, B. J. 2009, *Astron. J.*, **138**, 466.

Kwee, K. K., and Woerden, H. van 1956, *Bull. Astron. Inst. Netherlands*, **12**, 327.

Lucy, L. B. 1967, Z. Astrophys., **65**, 89.

Mateo, N. M., and Ruciński, S. M. 2017, *Astron. J.*, **154**, 125 (http://arxiv.org/abs/1708.01097v1).

Minor Planet Observer. 2015, MPO Canopus software (http://www.minorplanetobserver.com), BDW Publishing, Colorado Springs, CO.

Nelson, R. H. 2009, WDWINT version 5.6a astronomy software (https://www.variablestarssouth.org/bob-nelson).

O'Connell, D. J. K. 1951, *Publ. Riverview Coll. Obs.*, **2**, 85.

Pecaut, M. J., and Mamajek, E. E. 2013, *Astrophys. J., Suppl. Ser.*, **208**, 9.

Pojmański, G., Pilecki, B., and Szczygiel, D. 2005, *Acta Astron.*, **55**, 275.

Prša, A., and Zwitter, T. 2005, *Astrophys. J.*, **628**, 426.

Qian, S-B. 2003, Mon. Not. R. Astron. Soc., 342, 1260.

Qian, S.-B., He, J.-J., Soonthornthum, B., Liu, L., Zhu, L.-Y., Li, L.-J., Liao, W. P., and Dai, Z.-B. 2008, *Astron. J.*, **136**, 1940.

Qian, S.-B., and Yang, Y.-G. 2004, *Astron. J.*, **128**, 2430.

Qian, S.-B., and Yang, Y.-G. 2005, *Mon. Not. Roy. Astron. Soc.*, **356**, 765.

Ruciński, S. M. 1969, *Acta Astron.*, **19**, 245.

Schlafly, E. F., and Finkbeiner, D. P. 2011, *Astrophys. J.*, **737**, 103.

Schlegel, D. J., Finkbeiner, D. P., and Davis, M. 1998, *Astrophys. J.*, **500**, 525.

Schwarzenberg-Czerny, A. 1996, *Astrophys. J., Lett.*, **460**, L107.

Skelton, P. L., and Smits, D. P. 2009, *S. Afr. J. Sci.*, **105**, 120.

Software Bisque. 2013, THESKYX version 10.5.0 software (http://www.bisque.com).

Terrell, D., and Wilson, R. E. 2005, *Astrophys. Space Sci.*, **296**, 221.

Terrell, D., Gross, J., and Cooney, W. R. 2012, *Astron. J.*, **143**, 1.

Ulaş, B., Kalomeni, B. Keskin, V., Köse, O., and Yakut, K. 2012, *New Astron.*, **17**, 46.

van Hamme, W. 1993, *Astrophys. J.*, **106**, 2096.

Vanmunster, T. 2006, PERANSO v2.5, period analysis software (CBA Belgium Observatory http://www.peranso.com/).

Warner, B. 2007, *Minor Planet Bull.*, **34**, 113.

Watson, C., Henden, A. A., and Price, C. A. 2014, AAVSO International Variable Star Index VSX (Watson+, 2006–2014; http://www.aavso.org/vsx).

Wilson, R. E. 1990, *Astrophys. J.*, **356**, 613.

Wilson, R. E., and Devinney, E. J., 1971, *Astrophys. J.*, **166**, 605.

Wozniak, P. R., *et. al.* 2004, *Astron. J.*, **127**, 2436.

Yakut, K., and Eggleton, P. P. 2005, *Astrophys. J.*, **629**, 1055.

Yang, Y.-G., and Qian, S.-B. 2015, *Astron. J.*, **150**, 69.